NO_2 Sensing Properties of Macroporous In_2O_3-based Powders Fabricated by Utilizing Ultrasonic Spray Pyrolysis Employing Polymethylmethacrylate Microspheres as a Template

Takeo Hyodo[1,*], Hanako Inoue[1], Hitomi Motomura[1], Katsuhide Matsuo[1], Takeshi Hashishin[2], Jun Tamaki[2], Yasuhiro Shimizu[1], and Makoto Egashira[1]

[1]Department of Materials Science and Engineering, Faculty of Engineering, Nagasaki University, 1-14 Bunkyo-machi, Nagasaki 852-8521, Japan

[2]Department of Applied Chemistry, Faculty of Science and Engineering, Ritsumeikan University, Kusatsu-shi, Shiga 525-8577, Japan

*Corresponding author:

Takeo Hyodo, Dr.

Graduate School of Science and Technology, Nagasaki University

1-14 Bunkyo-machi, Nagasaki 852-8521, Japan

Tel: +81-95-819-2645

Fax: +81-95-819-2643

E-mail: hyodo@nagasaki-u.ac.jp

Abstract

Macroporous (mp-) In_2O_3-based microspheres as a NO_2 sensing material were prepared by pyrolysis of atomized $In(NO_3)_3$ aqueous solutions containing polymethylmethacrylate (PMMA) microspheres (150 nm in diameter) as a template. Well-developed spherical macropores (less than 100 nm in diameter) reflecting the morphology of the PMMA microsphere templates could be formed in the In_2O_3-based microspheres. The introduction of macropores into In_2O_3-based microspheres was very effective in improving the NO_2 response of their thick films fabricated on an alumina substrate equipped with interdigitated Pt electrodes (gap size: ca. 200 μm) by screen-printing. In addition, the addition of a little amount of SnO_2 to the mp-In_2O_3 microspheres not only lowered the resistance in air but also improved the NO_2 response. NO_2 sensing properties of non-stacked microspheres of the mp-In_2O_3 mixed with SnO_2 were also investigated by utilizing nano-gap Au electrodes (gap size: ca. 200 nm). The non-stacked microspheres showed fast response and recovery speeds to NO_2, because of better diffusion capability of NO_2.

***Keywords*:** Gas sensor; Indium oxide; Ultrasonic spray pyrolysis; Polymethylmethacrylate; Macropores

1. Introduction

Recently, numerous efforts have been directed to developing gas sensor materials with strictly-controlled nano- and micro-structures to improve their gas sensitivity and selectivity, because optimization of the size and the amount of pores in the gas sensor materials are very effective in controlling gas diffusivity and reactivity [1-6]. Therefore, we have so far developed different porous sensor materials by utilizing various techniques. For example, we have succeeded in preparing thermally stable mesoporous oxide powders by utilizing a self-assembly of a general surfactant such as *n*-cetylpyridinium chloride [7-11] or a triblockcopolymer such as $EO_{20}PO_{70}EO_{20}$ (EO: ethylene oxide, PO: propylene oxide, MW: ca. 5800) [12, 13] in an aqueous solution as a template. These materials showed excellent gas-sensing properties, due to their well-developed porous structure, extremely-high surface area and small crystallite size.

On the other hand, we have fabricated various macroporous (mp-) oxide films with submicron-sized spherical pores by a modified sol-gel technique [14-18], sputtering [19] and pulsed-laser deposition [20] employing a polymethylmethacrylate (PMMA) microsphere as a template, too. They were very effective in improving the gas sensing properties of various types of gas sensors such as semiconductor-type [14, 15, 20], solid electrolyte-type [18], quartz-crystal microbalance (QCM)-type [16] and fluorescence-type [17] gas sensors. Other groups have also focused on fabricating porous materials by utilizing polymer microspheres as a template and have investigated their gas sensing properties [21, 22]. However, it was quite difficult to control thickness of these mp-films by these techniques. Therefore, development of oxide powders with well-developed and submicron-sized macropores is now very necessary for easy fabrication of mp-oxide films by using some conventional fabrication processes such as screen-printing.

The ultrasonic spray pyrolysis is one of promising preparation techniques to fabricate

submicron-sized, uniform and spherical ceramic powders, and we have already succeeded in preparing hollow alumina microspheres by utilizing a general electric furnace [23] and microwave-induced plasma [24] as a reactor. Iskandar et al. have recently prepared mp-SiO_2 microspheres by thermal decomposition of atomized oxide precursor solutions containing polystyrene microspheres [25, 26]. We have also succeeded to prepare mp-SnO_2-based microspheres as a gas sensing material by an ultrasonic spray pyrolysis technique employing PMMA microspheres [27-29]. These well-developed porous morphology is very attractive as a raw material for various electrochemical devices such as fuel cells, batteries and chemical sensors. Actually, the mp-SnO_2 microspheres, which had well-developed spherical macropores reflecting the morphology of the PMMA microsphere template, showed relatively high H_2 and NO_2 sensing properties [27-29].

In this study, the effects of the introduction of macroporous structure into In_2O_3-based microspheres on NO_2 sensing properties have been investigated at 100~300°C in air, because it has been reported that In_2O_3 is an attractive NO_2-sensing material by various studies [30-33]. In addition, we have also tried to evaluate NO_2 sensing properties of non-stacked mp-In_2O_3-based microspheres by utilizing nano-gap Au electrodes [34-37].

2. Experimental

2.1 Preparation of mp-In_2O_3-based microspheres by ultrasonic spray pyrolysis

A given amount of PMMA microspheres of 150 nm in diameter (Soken Chem. & Eng. Co., Ltd.) were added to a 0.05 mol dm^{-3} $In(NO_3)_3$ aqueous solution and the mixtures were served as a precursor solution for the preparation of mp-In_2O_3 microspheres (mp-In_2O_3(P*m*), P means PMMA and *m* is the amount of PMMA microspheres dispersed in the solution (*10~30* g dm^{-3})) by ultrasonic spray pyrolysis. In some cases, $SnCl_4$ was added to the $In(NO_3)_3$ aqueous solution in order to prepare mp-In_2O_3 microspheres mixed with *n* mol% SnO_2

(mp-In_2O_3(P*30*)-*n*SnO_2, *n = 0.1* and *1.0* (mol%)) in order to improve the gas response as well as the conductivity. Conventional (c-) In_2O_3 and c-In_2O_3-*n*SnO_2 microspheres were also prepared by the similar preparation technique using a precursor aqueous solution containing no PMMA microspheres. All samples prepared in this study were summarized in Table 1. A specially-designed mist-supplier for the ultrasonic spray pyrolysis, which was used to get a uniform mist of the precursor solution, was shown in Fig. 1. Various sizes of mists of the precursor solution were generated in a plastic container equipped with a polyethylene thin film at one end, which was perpendicularly set over an ultrasonic vibrator (Honda Electric Co., Ltd., HM-303N, 2.4 MHz) at a distance of 0.5~1.0 cm in water. The mists were carried into a glass vessel by air flowing 1 (1.5 dm^3 min^{-1}), and only small droplets were allowed to move into an electric furnace heated at 1100°C with an assistance of air flowing 2 (1.5 dm^3 min^{-1}). Morphology of representative powders was observed by scanning electron microscopy (SEM; JEOL Ltd., JSM-7500F) and transmission electron microscopy (TEM; JEOL Ltd., JEM2010-HT). The specific surface area and pore size distribution were measured by BET and BJH methods using a N_2 adsorption isotherm (Micromeritics Inst. Corp., Tristar3000), respectively. Crystal phase was characterized by X-ray diffraction analysis (XRD; Rigaku Corp., RINT2200) using Cu Kα radiation (40 kV, 40 mA), and crystallite size was calculated from the (101) diffraction peak using Scherrer equation. The chemical states of all samples were characterized by X-ray photoelectron spectroscopy using Al Kα radiation (XPS, Kratos, AXIS-ULTRA DLD), and the binding energy was calibrated using the C 1s level from usual contamination (284.5 eV).

2.2 Fabrication of thick film sensors and measurement of their gas sensing properties

Thick film sensors were fabricated by screen-printing employing the paste of an oxide powder on an alumina substrate equipped with a pair of interdigitated Pt electrodes (gap size:

ca. 200 μm), followed by calcination at 550°C for 5 h. Gas response of these sensors was measured to 0.1~100 ppm NO_2 balanced with air in a flow apparatus at 100~300°C. The sensor obtained was connected in series with a reference resistance (R_R, 10^4~10^7 Ω) and a voltage (V_0, 2 V) was applied to them. The sensor resistance (R_S) was obtained by measuring the voltage drop of the reference resistance (V_R), using the following equation:

$$R_S = R_R\{(V_0/V_R)-1\} \quad (1)$$

The magnitude of response to NO_2 was defined as the ratio (R_g/R_a) of sensor resistance after 10 min in NO_2 (R_g) balanced with air to that in air (R_g).

3. Results and Discussions

3. 1 Characterization of c-In_2O_3 and mp-In_2O_3 microspheres

Figure 2 shows SEM and TEM photographs of c-In_2O_3 and c-In_2O_3-*1.0*SnO_2 microspheres prepared without PMMA microspheres. Both the powders are roughly-spherical with 100~500 nm in diameter, and a TEM photograph of the c-In_2O_3 microsphere (Fig. 2(a)(ii)) shows that the bulk was exactly dense. In contrast, the size of all mp-In_2O_3(P*m*) microspheres (250~1500 nm in diameter) is much larger than that of the c-In_2O_3 and c-In_2O_3-*1.0*SnO_2 microspheres and many spherical macropores of less than 100 nm in diameter were observed on the surface, as shown in Fig. 3. The morphology of their macropores reflects that of PMMA microspheres, but the size indicates a large shrinkage of voids originating from PMMA microspheres which were about 150 nm in diameter. In addition, the amount of spherical macropores tended to increase with an increase in the amount of PMMA microspheres added in the precursor solution, and the inner structure of the mp-In_2O_3(P*30*) microsphere, which was prepared from the precursor solution containing a

largest amount of PMMA microspheres, are pretty similar to that of "sponge" made of polyurethane (see the high-resolution image of Fig. 3(c)). On the other hand, the mixing of 1.0 mol% SnO_2 to the mp-In_2O_3(P*30*) powder made little important change to the inner structure (morphology and size of macropores) as shown in Fig. 3(d), while the size of the mp-In_2O_3(P*30*)-*1.0*SnO_2 microsphere was smaller than that of the mp-In_2O_3(P*30*) microsphere. Figure 4 shows TEM photographs of an mp-In_2O_3(P*30*) microsphere. All spherical macropores were well-developed inside the microspheres and continuously connected each other. XRD patterns of all samples showed that the structure of all samples was cubic and any impurities were not confirmed even in those of c- and m-In_2O_3(P*30*)-*1.0*SnO_2 microspheres (no data is shown here). The crystallite size calculated by using Scherrer equation from the XRD spectrum of the mp-In_2O_3(P*30*) microsphere was ca. 38.8 nm. Considering the crystallite size, each oxide wall between the macropores seem to consist of only a few crystallites, probably because oxide precursors were separated among PMMA microspheres and then they were pyrolyzed and subsequently sintered at elevated temperatures at the limited region after the decomposition of PMMA microspheres. Figure 5 shows pore size distributions of representative c- and mp-In_2O_3-based microspheres, together with their specific surface area (SSA) and crystallite size (CS) obtained from their XRD spectra. The CS of mp-In_2O_3(P*30*) or mp-In_2O_3(P*30*)-*1.0*SnO_2 (38.8 nm or 37.6 nm, respectively) was apparently small than that of c-In_2O_3 or c-In_2O_3-*1.0*SnO_2 (46.9 nm and 56.4 nm, respectively). Assuming that the morphology of their crystallites with the density of 7.180 g cm^{-3} [38] is spherical, the geometric surface area (GSA) of mp-In_2O_3(P*30*) and mp-In_2O_3(P*30*)-*1.0*SnO_2 microspheres, which was calculated from the density and the CS obtained from their XRD spectra, was 21.0 and 22.2 m^2 g^{-1}, respectively. This value was only a little larger than GSA of c-In_2O_3 and c-In_2O_3-*1.0*SnO_2 (16.4 and 14.6 m^2 g^{-1}, respectively), which was calculated in the same way. Experimental SSA value of

mp-In_2O_3(P*30*) and mp-In_2O_3(P*30*)-*1.0*SnO_2 (23.4 or 21.8 m^2 g^{-1}, respectively), which was measured by a BET method using N_2 adsorption, was comparable to their GSA values, while that of c-In_2O_3 and c-In_2O_3-*1.0*SnO_2 (2.26 and 2.58 m^2 g^{-1}, respectively) was much smaller than their GSA values. In addition, mp-In_2O_3(P*30*) and mp-In_2O_3(P*30*)-*1.0*SnO_2 had much larger pore volume (less than ca. 10 nm in diameter) than c-In_2O_3 and c-In_2O_3-*1.0*SnO_2, as shown in Fig. 5. These results show that microsphere of mp-In_2O_3(P*30*) and mp-In_2O_3(P*30*)-*1.0*SnO_2 had not only well-developed macropores (see Figs. 3 and 4) but also well-developed nanopores and mesopores among their crystallites. On the other hand, c-In_2O_3 and c-In_2O_3-*1.0*SnO_2 had extremely small pore volume, and the diameter of c-In_2O_3 and c-In_2O_3-*1.0*SnO_2 microspheres, which were calculated with the experimental SSA value, was 370 nm and 324 nm, respectively, which are almost comparable with that of their actual microspheres, as shown in Fig. 2. These results support that their microspheres of c-In_2O_3 and c-In_2O_3-*1.0*SnO_2 are extremely dense.

XPS spectra of Sn 3d of mp-In_2O_3(P*30*)-*0.1*SnO_2, mp-In_2O_3(P*30*)-*1.0*SnO_2 and c-In_2O_3-*1.0*SnO_2 are shown in Fig. 6. Typical spectra originating from SnO_2 were observed, and the binding energy (ca. 487.2 and ca. 495.7 eV for Sn $3d_{5/2}$ and $3d_{3/2}$, respectively) are independent on the microstructure and the additive amount of SnO_2. XPS spectra of other elements (In and O) of all samples were measured, but their binding energy are not also dependent on the microstructure and the additive amount of SnO_2 at all (no data is shown here).

3. 2 NO_2 sensing properties of mp-In_2O_3 sensors

Figure 7 shows response transients of mp-In_2O_3(P*30*) and c-In_2O_3 sensors to 10 ppm and 100 ppm NO_2 in air at 250°C. The response and recovery speeds of mp-In_2O_3(P*30*) are much faster than those of c-In_2O_3. A little amount of nanopores less than ca. 2 nm in

diameter (the diameter range of "micropores" in the classification proposed by the International Union of Applied Chemistry) only exist in the submicron-sized c-In_2O_3 microspheres, as shown in Figs. 2 and 5. In the nano-space, surface diffusion in the nanopores, which is based on the interaction between molecules and the pore surface, is a main dominant factor to determine the molecular transfer rate in the pores, and thus the gas-diffusion coefficient is much lower than that in the mesopores (2~50 nm) [39]. On the other hand, mp-In_2O_3(P*30*) microsphere have a large amount of mesopores where Knudsen diffusion is dominant (see Fig. 5), together with well-developed macropores in molecular diffusion region (see Figs. 3 and 4). This is the reason for much faster response and recovery speeds observed for mp-In_2O_3(P*30*) than c-In_2O_3. In addition, the magnitude of response of mp-In_2O_3(P*30*) was larger than that of c-In_2O_3. Operating temperature dependence of the magnitude of response to 10 ppm NO_2 of all mp-In_2O_3(P*m*) and c-In_2O_3 sensors is shown in Fig. 8. In this figure, each response value was calculated at 10 min later after the introduction of 10 ppm NO_2, although steady-state response could not be obtained within 10 min exposure under the present experimental conditions. The magnitude of response of c-In_2O_3 was extremely small, because of the extremely small SSA value. In addition, the response decreased with an decrease in operating temperature, because only a small amount of nanopores with a diameter of less than 2 nm formed inside the c-In_2O_3 microspheres and thus the diffusion of NO_2 at the surface of all crystallites inside the microsphere at lower temperatures was undoubtedly slower than that at higher temperatures. On the other hand, at 300°C, which is the highest operating temperature, the magnitude of response of mp-In_2O_3(P*m*) was comparable with that of c-In_2O_3. The magnitude of response of mp-In_2O_3(P*m*) with large SSA and well-developed macropores was much larger than that of c-In_2O_3 at lower temperatures. In addition, their magnitude of response tends to increase with an increase in the amount of macropores, probably because the large porous structure has

the important effects on the diffusion of NO_2.

As mentioned above, mp-In_2O_3(P*m*) sensors showed a large response to NO_2 at lower temperatures, but their resistance in NO_2 balanced with air was too high for their practical applications. Therefore, we tried to dope a little amount of SnO_2 into In_2O_3 in order to reduce the film resistance. Figure 9 shows response transients of mp-In_2O_3(P*30*)-*n*SnO_2 (*n* = 0.1 and 1.0) sensors to 10 ppm NO_2 in air at 100 and 250°C, together with that of an mp-In_2O_3(P*30*) sensor. The sensor resistance in air apparently decreased with an increase in the amount of SnO_2 addition. In addition, the sensor resistances of mp-In_2O_3(P*30*) and mp-In_2O_3(P*30*)-*0.1*SnO_2 in air at 100°C are much larger than those at 250°C, while the sensor resistance of mp-In_2O_3(P*30*)-*1.0*SnO_2 in air at 100°C are comparable with that at 250°C. These results implied that SnO_2 was doped into the In_2O_3 lattice of mp-In_2O_3(P*30*) and the concentration of free electrons was extremely large in mp-In_2O_3(P*30*)-*1.0*SnO_2. On the other hand, the doping of SnO_2 to mp-In_2O_3(P*30*) induced little effect in improving the magnitude of response at 250°C, while the magnitude of response of mp-In_2O_3(P*30*)-*n*SnO_2 at 100°C was much larger than that of mp-In_2O_3(P*30*). Since SSA (20.2 and 21.8 m^2 g^{-1}), CS (41.8 and 37.6 nm) and pore-size distribution of mp-In_2O_3(P*30*)-*0.1*SnO_2 and mp-In_2O_3(P*30*)-*0.1*SnO_2 are comparable with those of mp-In_2O_3(P*30*), the improvement of recovery speed of mp-In_2O_3(P*30*)-*0.1*SnO_2 and mp-In_2O_3(P*30*)-*0.1*SnO_2 may be ascribed to the change in surface properties induced by the doping of SnO_2 to In_2O_3.

Figure 10 shows NO_2 concentration dependence of response of macroporous sensors (mp-In_2O_3(P*30*) and mp-In_2O_3(P*30*)-*1.0*SnO_2) and conventional sensors (c-In_2O_3 and c-In_2O_3-*1.0*SnO_2) at 250ºC. In every concentration range, NO_2 response of macroporous samples are higher than those of conventional sensors, and the NO_2 sensitivity (i.e., the slope of the line) of mp-In_2O_3(P*30*)-*1.0*SnO_2 is larger than that of mp-In_2O_3(P*30*). The linearity between the response and NO_2 concentration was confirmed in a lower NO_2 concentration

range tested, but the response to NO_2 has a tendency to saturate in a higher NO_2 concentration range.

3. 3 NO_2 sensing properties of non-stacked mp-In_2O_3(P*30*)-*1.0*SnO_2 microspheres by utilizing nano-gap Au electrodes

NO_2 sensing properties of non-stacked mp-In_2O_3(P*30*)-*1.0*SnO_2 microspheres were also tested by utilizing nano-gap Au electrodes. Figure 11 shows the schematic drawing and actual photograph of the nano-gap Au electrodes on a glass substrate. The distance between Au electrodes (ca. 300 nm in thickness and ca. 10 μm in width) is ca. 200 nm. Thus, it is expected that some mp-In_2O_3(P*30*)-*1.0*SnO_2 microspheres could be loaded between the electrodes without stacking the particles, by dripping a dispersion containing a little amount of mp-In_2O_3(P*30*)-*1.0*SnO_2 microspheres at the gap between Au electrodes. Experimentally, ca. 10 mg of mp-In_2O_3(P*30*)-*1.0*SnO_2 microspheres was dispersed in 10 cm^3 of deionized water, and then the small amount of the dispersion was dripped onto the nano-gap Au electrodes. After dried at RT and then heat-treated at 300°C in air, the non-stacked microsphere sensor with nano-gap Au electrodes was obtained. Figure 12 shows SEM photographs of the surface of nano-gap Au electrodes attached with and without mp-In_2O_3(P*30*)-*1.0*SnO_2 microspheres, together with that of the cross-section of a thick film sensor fabricated by screen-printing employing mp-In_2O_3(P*30*)-*1.0*SnO_2 microspheres. The nano-gap which was formed by a focused ion beam was confirmed clearly (Fig. 12(a)), while a part of the nano-gap electrodes was peeled off by several immersions of the aqueous dispersion. After loading the mp-In_2O_3(P*30*)-*1.0*SnO_2 microspheres, they were set between the Au electrodes independently without stacking, as shown in Fig. 12(b). Figure 13 shows response transients to 1.0 ppm NO_2 of the non-stacked microsphere sensor and the thick film sensor of mp-In_2O_3(P*30*)-*1.0*SnO_2. The sensor resistance of the non-stacked microsphere

sensor was quite higher than that of the thick film sensor, because of too few electrical contact points, while the magnitude of response of the non-stacked microsphere sensor was smaller than that of the thick film sensor. On the other hand, the response and recovery speeds of the non-stacked microsphere sensor were much faster than those of the thick film sensor, because of a large difference in the morphology of gas-sensitive region (oxide) between both sensors. Figure 14 shows schematic drawings of gas diffusion behavior in the non-stacked microsphere sensor and the thick film sensor. The oxide thickness of the non-stacked microsphere sensor was the diameter of macroporous particle, less than 1 μm, while that of the thick film sensor was ca. 4 μm. Therefore, the time interval required for gaseous molecules to reach to the main region determining the sensor resistance (the bottom of the oxide layer) of the non-stacked microsphere sensor is much shorter than that of the thick film sensor. In addition, gaseous molecules can easily and swiftly get through the inner region of an mp-microsphere between Au electrodes, in case of the non-stacked microsphere sensor. Therefore, the gas diffusion rate in the non-stacked microsphere sensor is expected to be much faster than that in the thick film sensor. Such difference of gas-diffusion rate between both sensors has a large influence on their response and recovery behavior. Further structural control of the gas-sensitive region, i.e. the morphological optimization of nano-gap Au electrodes as well as macropores and nanopores in the oxide microsphere, will offer drastic improvement in gas-sensing properties to the non-stacked microsphere sensor.

4. Conclusion

Spherical mp-In_2O_3(P*m*) and mp-In_2O_3(P*30*)-*n*SnO_2 microspheres were prepared by ultrasonic spray pyrolysis of atomized $In(NO_3)_3$ aqueous solutions containing PMMA microspheres as a template and their NO_2 sensing properties were investigated at 100~300°C. A c-In_2O_3 microsphere which was prepared without PMMA microspheres was exactly dense,

while all mp-In_2O_3(P*m*) microspheres are much larger than that of the c-In_2O_3 powder and well-developed spherical macropores of less than 100 nm in diameter, which reflected the morphology of the PMMA microsphere templates, were formed in the mp-In_2O_3(P*m*) microspheres. The NO_2 responses of mp-In_2O_3(P*m*) thick films showed much larger response and fast response and recovery speeds than those of c-In_2O_3 thick films, because excellent gas-diffusion properties in the well-developed macroporous structure. In addition, the addition of a little amount of SnO_2 to the mp-In_2O_3 microspheres not only lowered the resistance but also improved the NO_2 response. A non-stacked mp-In_2O_3(P*30*)-*1.0*SnO_2 microsphere sensor which was fabricated by utilizing nano-gap Au electrodes showed significantly fast response and recovery speeds to NO_2, because the NO_2 diffusion was drastically improved.

References

1. G. Sakai, N. Matsunaga, K. Shimanoe, N. Yamazoe, Theory of Gass-diffusion Controlled Sensitivity for Thin Film Semiconductor Gas Sensor, Sens. Actuators B, 80 (2001) 125-131.
2. M. Tiemann, Porous Metal Oxides as Gas Sensors, Chem. Eur. J., 13 (2007) 8376-8388.
3. N. Yamazoe, New Perspectives of Gas Sensor Technology, Sens. Actuators B, 138 (2009) 100-107.
4. T. Wagner, T. Sauerwald, C.-D. Kohl, T. Waitz, C. Weidmann, M. Tiemann, Gas Sensor based on Ordered Mesoporous In_2O_3, Thin Solid Films, 517 (2009) 6170-6175.
5. D. Wang, P. Hu, J. Xu, X. Dong, Q. Pan**,** Fast Response Chlorine Gas Sensor Based on Mesoporous SnO_2, Sens. Actuators B, 140 (2009) 383-389.
6. C.-Y. Liu, C.-F. Chen, J.-P. Leu, Tunable Interconnectivity of Mesostructured Cobalt Oxide Materials for Sensing Applications, Sens. Actuators B, 137 (2009) 700-703.
7. T. Hyodo, N. Nishida, Y. Shimizu, M. Egashira, Preparation and gas-sensing properties of thermally stable mesoporous SnO_2, Sens. Actuators B, 83 (2002) 209-215.
8. G. S. Devi, T. Hyodo, Y. Shimizu, M. Egashira, Synthesis of Mesoporous TiO_2-based Powders and their Gas-Sensing Properties, Sens. Actuators B 87 (2002) 122-129.
9. T. Hyodo, S. Abe, Y. Shimizu, M. Egashira, Gas-sensing properties of ordered mesoporous SnO_2 and effects of coatings thereof, Sens. Actuators B 93 (2003) 590-600.
10. C. Yu, T. Hyodo, Y. Shimizu, M. Egashira, Preparation of Thermally Stable Mesoporous TiO_2 Powder and its Gas Sensor Application, Electrochemistry, Electrochemistry 71 (2003) 475-480.
11. M. Hayashi, T. Hyodo, Y. Shimizu, M. Egashira, Effects of Microstructure of Mesoporous SnO_2 Powders on Their H_2 Sensing Properties, Sens. Actuators B 141 (2009) 465-470.
12. Y. Shimizu, A. Jono, T. Hyodo, M. Egashira, Preparation of Large Mesoporous SnO_2

Powder for Gas Sensor Application, Sens. Actuators B 108 (2005) 56-61.

13. T. Hyodo, K. Murayama, Y. Shimizu, M. Egashira, Large Mesoporous Tin Dioxide Powders for Gas Sensor Materials -Effects of Various Additives on the Mesostructure and the H_2 Sensing Properties-, Rare Metal Mater. & Eng. 35, Suppl. 3 (2006) 455-458.
14. T. Hyodo, K. Sasahara, Y. Shimizu, M. Egashira, Preparation of macroporous SnO_2 films using PMMA microspheres and their sensing properties to NOx and H_2, Sens. Actuators B 106, (2005) 580-590.
15. S. Nonaka, T. Hyodo, Y. Shiimizu, M. Egashira, Preparation of macroporous semiconductor gas sensors and their odur sensing properties, IEEJ Trans. SM 128 (2008) 141-144.
16. H. Seh, T. Hyodo, H. L. Tuller, Bulk Acoustic Wave Resonator as a sensing platform for NOx at high temperatures, Sens. Actuators B 108, (2005) 547-552.
17. Y. Takakura, T. Hyodo, Y. Shiimizu, M. Egashira, Preparation of macroporous Eu-doped oxide thick films and their application to gas sensor materials, IEEJ Trans. SM 128 (2008) 137-140.
18. M. Morio, T. Hyodo, Y. Shiimizu, M. Egashira, Effect of Macrostructural Control of an Auxiliary Layer on the CO_2 Sensing Properties of NASICON-based Gas Sensors, Sens. Actuators B 139 (2009) 563-569.
19. T. Hyodo, A. Bieberle-Hütter, J. L. Hertz, H. L. Tuller, Three Dimensional Arrays of Hollow Gadolinia-doped Ceria Microspheres Prepared by R.F. Magnetron Sputtering Employing PMMA Microsphere Templates, J. Electroceramics 17 (2006) 695-699.
20. I.-D. Kim, A. Rothschild, T. Hyodo, H. L. Tuller, Microsphere Templating as Means of Enhancing Surface Activity and Gas Sensitivity of $CaCu_3Ti_4O_{12}$ Thin Films, Nano Letters 6 (2006) 193 -198.
21. C. J. Martinez, B. Hockey, C. B. Montgomery, S. Semancik, Porous Tin Oxide

Nanostructured Microspheres for Sensor Applications, Langmuir 21 (2005) 7937-7944.

22. I.-D. Kim, A. Rothschild, D.-J. Yang, H. L. Tuller, Macroporous TiO_2 Thin Film Gas Sensors Obtained Using Colloidal Templates, Sens. Actuators B 130 (2008) 9-13.
23. T. Kato, M. Tashiro, K. Sugimura, T. Hyodo, Y. Shimizu, M. Egashira, Preparation of Hollow Alumina Microspheres by Ultrasonic Spray Pyrolysis, J. Ceram. Soc. Jpn 110 (2002) 146-148.
24. T. Hyodo, M. Murakami, Y. Shimizu, M. Egashira, Preparation of Hollow Alumina Microspheres by Microwave-induced Plasma Pyrolysis of Atomized Precursor Solution, J. Eur. Ceram. Soc. 25 (2005) 3563-3572.
25. F. Iskandar, Mikrajuddin, K. Okuyama, In Situ Production of Spherical Silica Particles Containing Self-organized Mesopores, Nano Lett. 1 (2001) 231-234.
26. F. Iskandar, Mikrajuddin, K. Okuyama, Controllability of Pore Size and Porosity on Self-organized Porous Silica Particles, Nano Lett. 2 (2002) 389-392.
27. K. Hieda, T. Hyodo, Y. Shimizu, M. Egashira, Preparation of Porous Tin Dioxide Powder by Ultrasonic Spray Pyrolysis and Their Application to Sensor Materials, Sens. Actuators B 133 (2008) 144-150.
28. M. Hashimoto, H. Inoue, T. Hyodo, Y. Shimizu, M. Egashira, Preparation and Gas Sensor Application of Ceramic Particles with Submicron-Size Spherical Macropores, Sensor Lett. 6 (2008) 887-890.
29. A. Anaraki Firooz, T. Hyodo, A. R. Mahjoub, A. A. Khodadadi, Y. Shimizu, Synthesis of Nano- and Meso-porous MoO_3-doped SnO_2 as a Selective Gas-sensing Material to NO_2, Sens. Actuators B, submitted.
30. A. Gurlo, N. Bârsan, M. Ivanovskaya, U. Weimar, W. Göpel , In_2O_3 and MoO_3–In_2O_3 Thin Film Semiconductor Sensors: Interaction with NO_2 and O_3, Sens. Actuators B 47 (1998) 92-99.

31. H. Steffes, C. Imawan, F. Solzbacher, E. Obermeier, Enhancement of NO_2 Sensing Properties of In_2O_3-based Thin Films Using an Au or Ti Surface Modification, Sens. Actuators B 78 (2001) 106-112.
32. L. Francioso, A. Forleo, S. Capone, M. Epifani, A. M. Taurino, P. Siciliano, Nanostructured In_2O_3–SnO_2 Sol–gel Thin Film as Material for NO_2 Detection, Sens. Actuators B 114 (2006) 646-655.
33. D. Chu, Y.-P. Zeng, D. Jiang and Y. Masuda, In_2O_3-SnO_2 Nano-toasts and Nanorods: Precipitation Preparation, Formation Mechanism, and Gas Sensitive Properties, Sens. Actuators B 137 (2009) 630-636.
34. J. Tamaki, A. Miyaji, J. Makinodan, S. Ogura, S. Konishi, Effect of Micro-gap Electrode on Detection of Dilute NO_2 Using WO_3 Thin Film Microsensors, Sens. Actuators B 108 (2005) 202-206.
35. J. Tamaki, J. Niimi, S. Ogura, S. Konishi, Effect of Micro-gap Electrode on Sensing Properties to Dilute Chlorine Gas of Indium Oxide Thin Film Microsensors, Sens. Actuators B 117 (2006) 353-358.
36. J. Tamaki, Y. Nakataya, S. Konishi, Micro Gap Effect on Dilute H_2S Sensing Properties of SnO_2 Thin Film Microsensors, Sens. Actuators B 130 (2008) 400-404.
37. J. Tamaki, T. Hashishin, Y. Uno, D. V. Dao, S. Sugiyama, Ultrahigh-sensitive WO_3 Nanosensor with Interdigitated Au Nano-electrode for NO_2 Detection, Sens. Actuators B 132 (2008) 234-238.
38. The Merck Index, 14th Ed., Ed. by M. J. O'Neil, Merck & Co., Inc., p. 860 (2006).
39. R. M. A. Roque-Malherbe, Adsorption and Diffusion in Nanoporous Materials, CRC Press, pp. 121-166 (2007).

Biographies

Takeo Hyodo received his B. Eng. Degree in applied chemistry and M. Eng. Degree in materials science and technology in 1992 and 1994, respectively, and Dr. Eng. Degree in 1997 from Kyushu University. He has been an assistant professor at Nagasaki University since 2007. His research interests are the developments of electrochemical devices such as chemical sensors and lithium batteries, and mesoporous and macroporous materials.

Hanako Inoue received his B. Eng. Degree in materials science and engineering from Nagasaki Uniersity in 2007.

Hitomi Motomura received his B. Eng. Degree and M. Eng. Degree in materials science and engineering from Nagasaki Uniersity in 2008.

Katsuhide Matsuo has been a technical staff at Nagasaki Uniersity since 1971.

Takeshi Hashishin received the BS degree in 1996 in Engineering from Ryukoku University, and the MS degree in 1998 and the PhD degree in 2000 in Materials Engineering from Ritsumeikan University. He is currently an assistant professor in Ritsumeikan University. His research interests include nanomaterials-synthesis based on carbon or oxide by using chemical vapor deposition and electrochemical treatment for application to chemically or mechanically sensing device.

Jun Tamaki has been a professor at Ritsumeikan University since 2002. He received the B Eng degree in chemical engineering in 1983 and the Dr Eng degree in 1988 from Osaka University. His current research interests include semiconductor gas sensors, synthesis of oxide thin film by solution process, synthesis and application of nano-structured materials, and heterogeneous catalysts.

Yasuhiro Shimizu received his B. Eng. Degree in applied chemistry in 1980 and Dr. Eng. Degree in 1987 from Kyushu University. He has been a professor at Nagasaki University

since 2005. His current research concentrates on development of odor sensors and design of intelligent sensors by controlling gas diffusivity and reactivity.

Makoto Egashira received his B. Eng. Degree and M. Eng. Degree in applied chemistry in 1966 and 1968, respectively, and Dr. Eng. Degree in 1974 from Kyushu University. He was a professor at Nagasaki University from 1985 to 2009, and now an emeritus professor at Nagasaki University. His current interests include the development of new chemical sensors, surface modification of ceramics, preparation of hollow ceramic microspheres and porous films and application of microwave-induced plasma.

Figure Captions

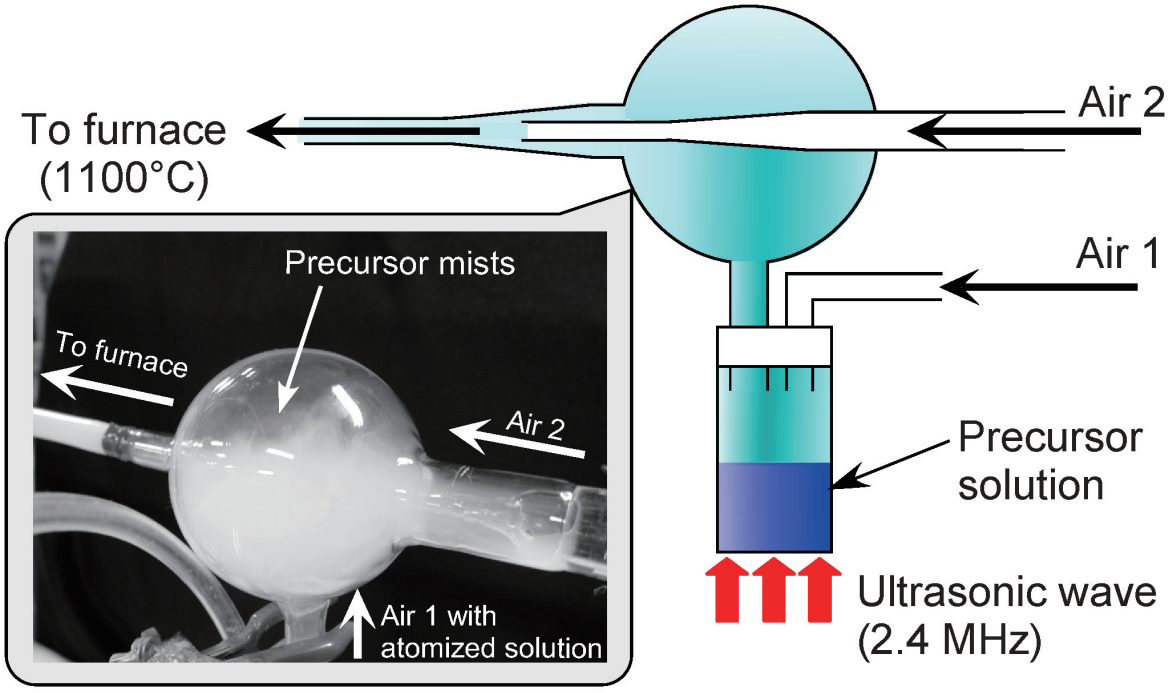

Fig. 1. Schematic drawing of a feeding system of a precursor solution atomized by ultrasonication (2.4 MHz).

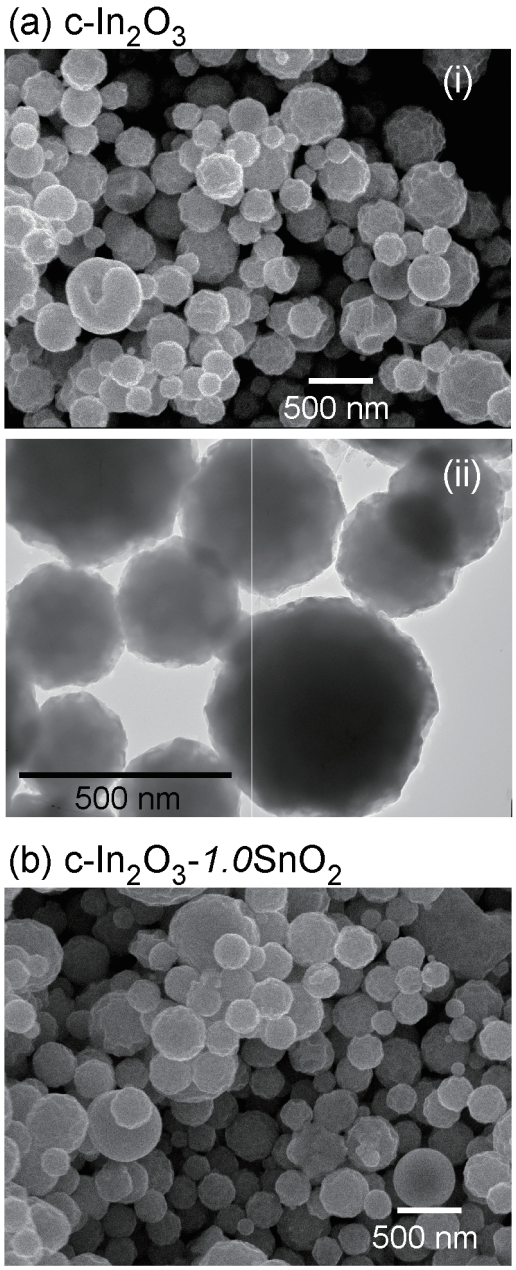

Fig. 2. SEM and TEM photographs of (a) c-In_2O_3 and (b) c-In_2O_3-*1.0*SnO_2 microspheres prepared without PMMA microspheres.

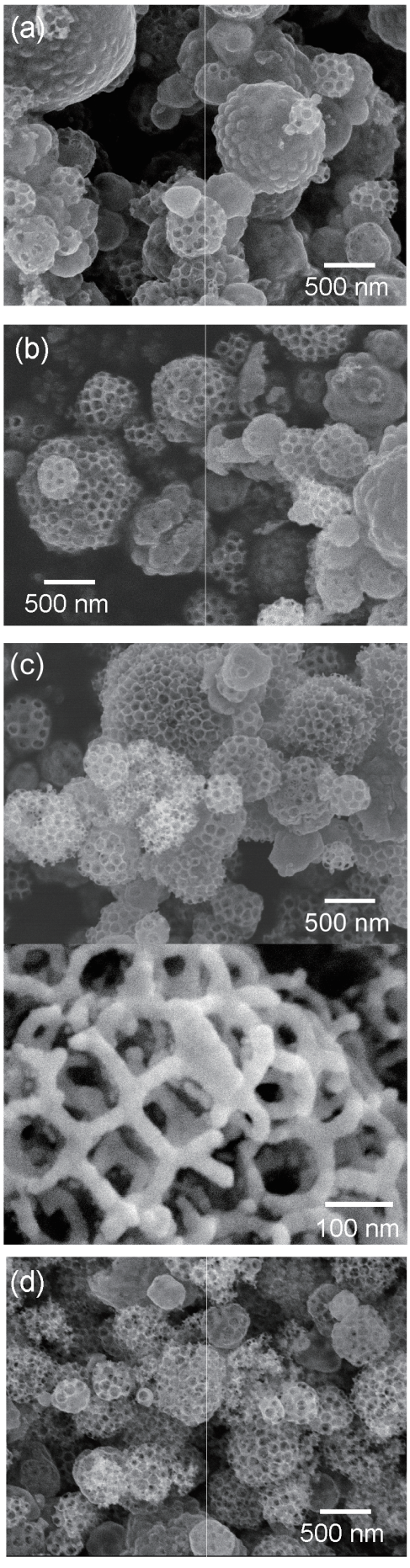

Fig. 3. SEM photographs of mp-In_2O_3(P*m*) (*m* = (a) *10*, (b) *20* and (c) *30*) and (d) mp-In_2O_3(P*30*)-*1.0*SnO_2 microspheres.

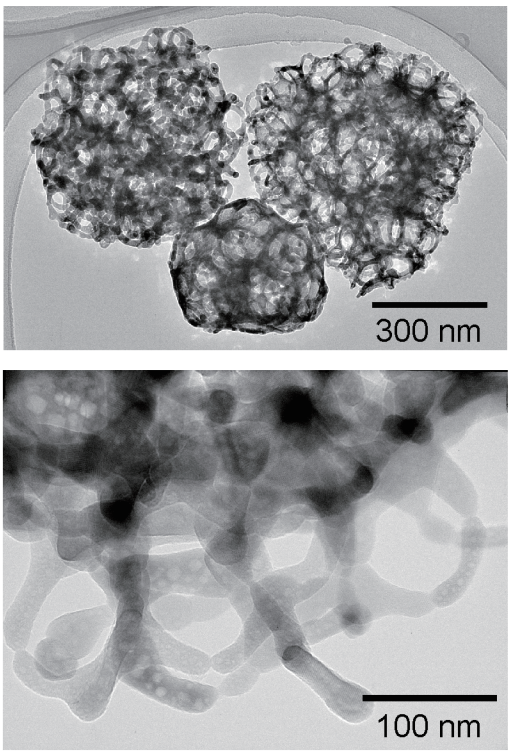

Fig. 4. TEM photographs of an mp-In_2O_3(P*30*) microsphere.

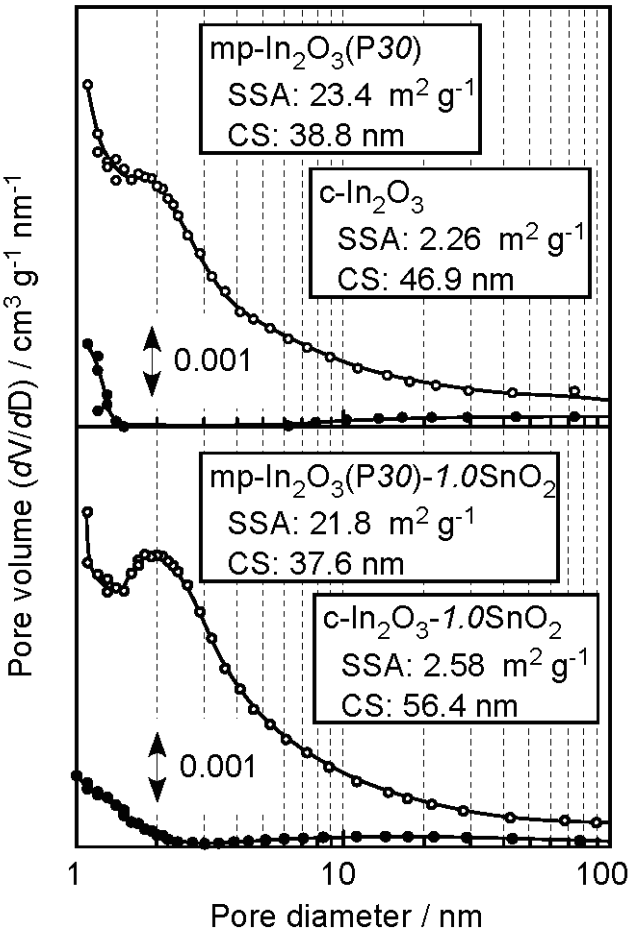

Fig. 5. Pore size distributions of representative c- and mp-In_2O_3-based microspheres, together with their specific surface area (SSA) and crystallite size (CS) obtained from their XRD spectra.

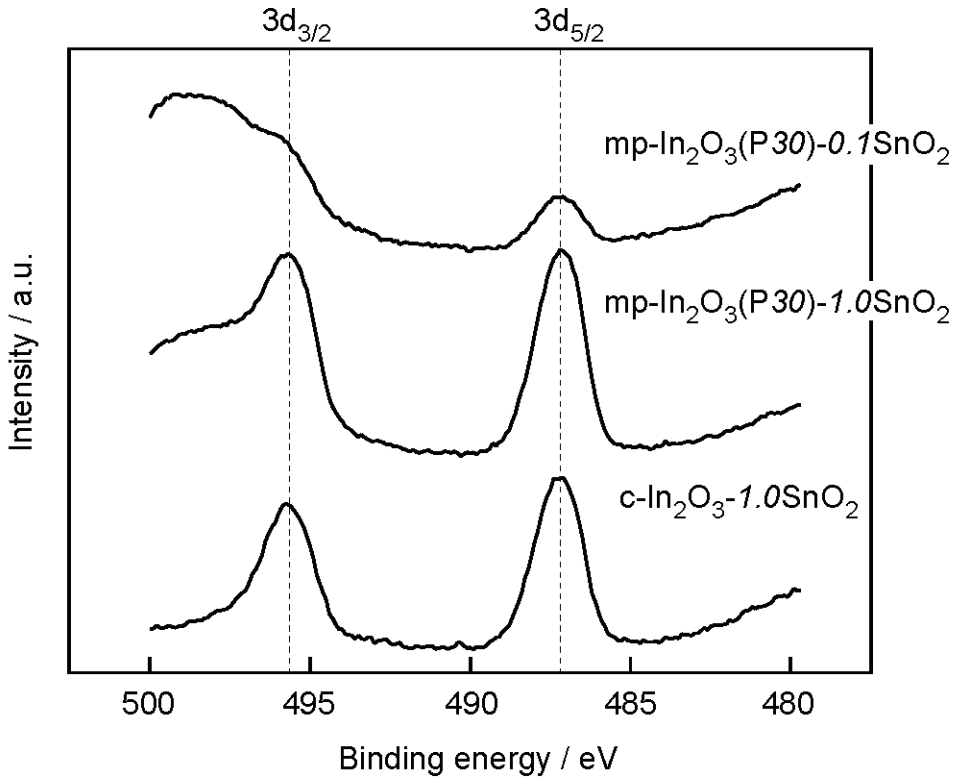

Fig. 6. XPS spectra of Sn 3d of mp-In_2O_3(P*30*)-*0.1*SnO_2, mp-In_2O_3(P*30*)-*1.0*SnO_2 and c-In_2O_3-*1.0*SnO_2.

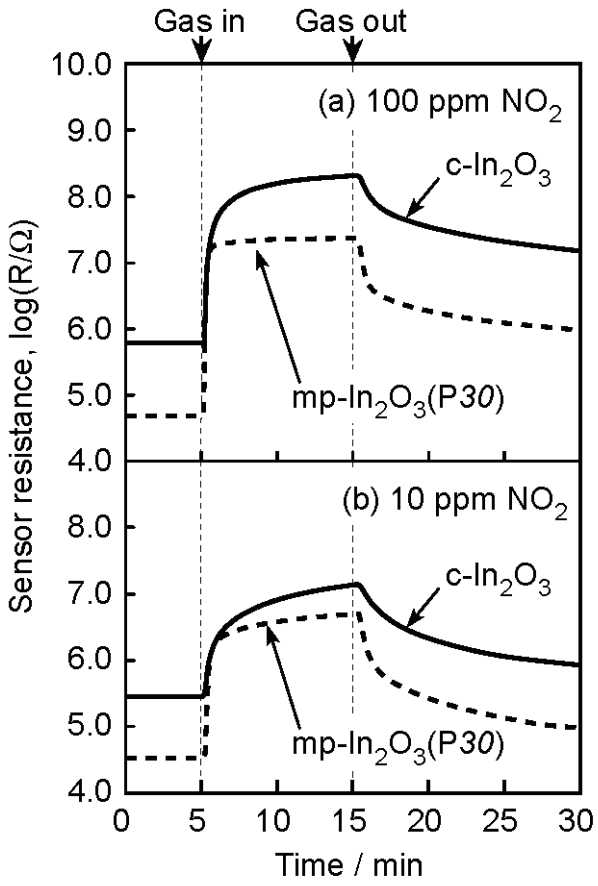

Fig. 7. Response transients of c-In_2O_3 and mp-In_2O_3(P*30*) sensors to 10 ppm and 100 ppm NO_2 in air at 250°C.

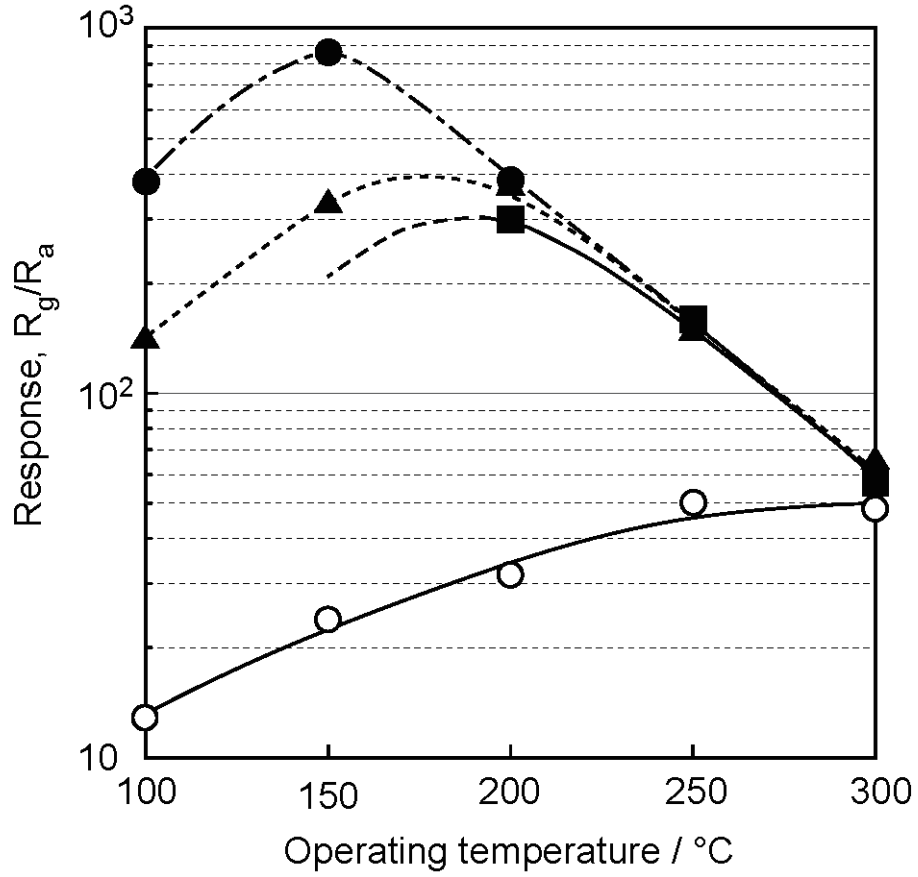

Fig. 8. Operating temperature dependence of the magnitude of response to 10 ppm NO_2 of all mp-In_2O_3(P*m*) and c-In_2O_3 sensors.

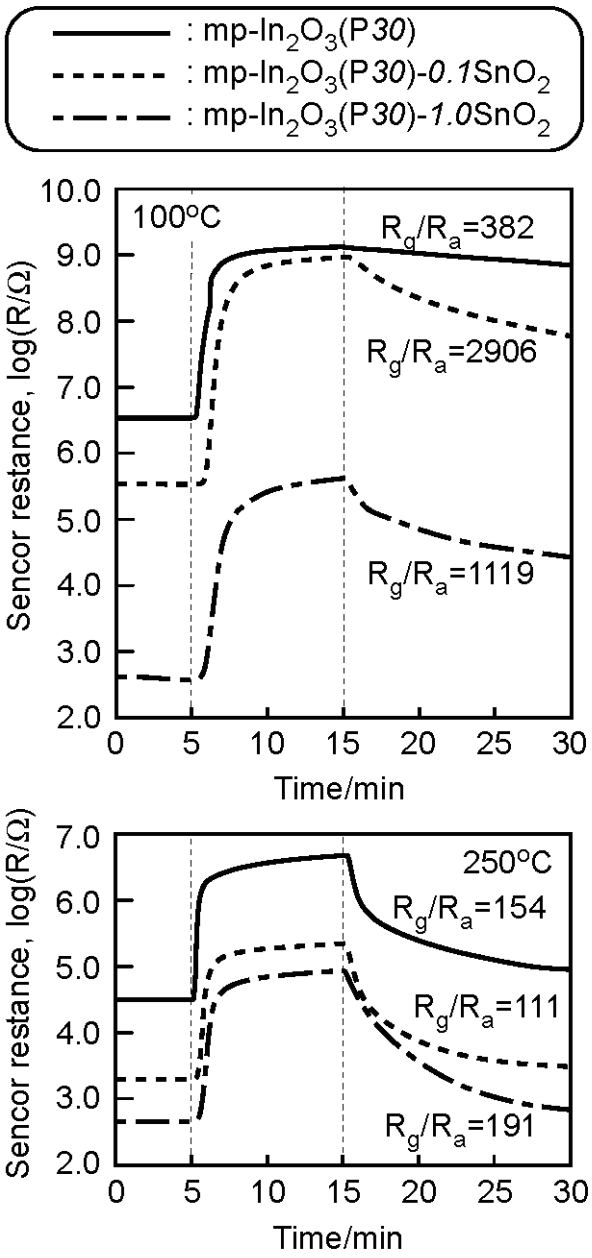

Fig. 9. Response transients of mp-In_2O_3(P*30*) and mp-In_2O_3(P*30*)-*n*SnO_2 (*n* = 0.1 and 1.0) sensors to 10 ppm NO_2 in air at 100 and 250°C.

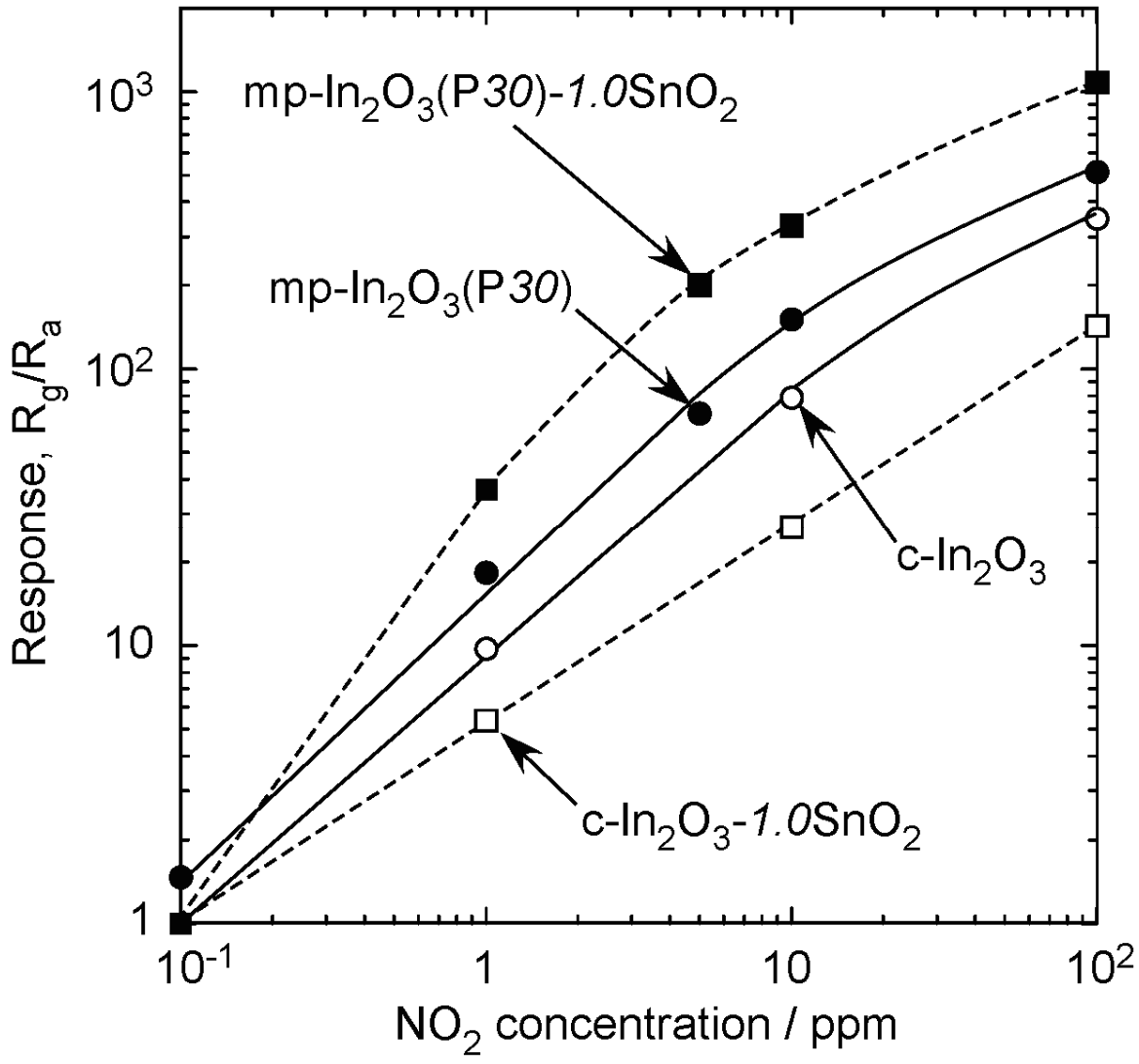

Fig. 10. NO_2 concentration dependence of responses of macroporous sensors (mp-In_2O_3(P*30*) and mp-In_2O_3(P*30*)-*1.0*SnO_2) and conventional sensors (c-In_2O_3 and c-In_2O_3-*1.0*SnO_2) at 250ºC.

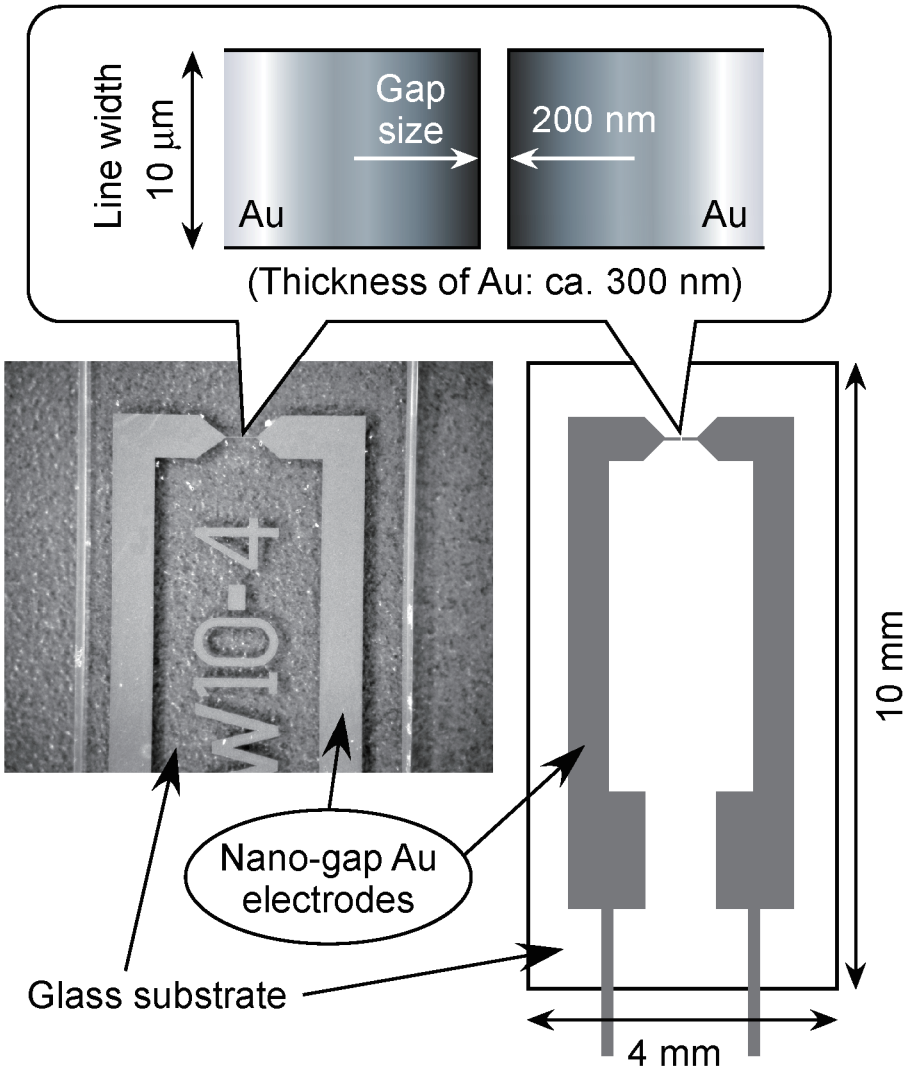

Fig. 11. Schematic drawing and photograph of nano-gap Au electrodes on a glass substrate.

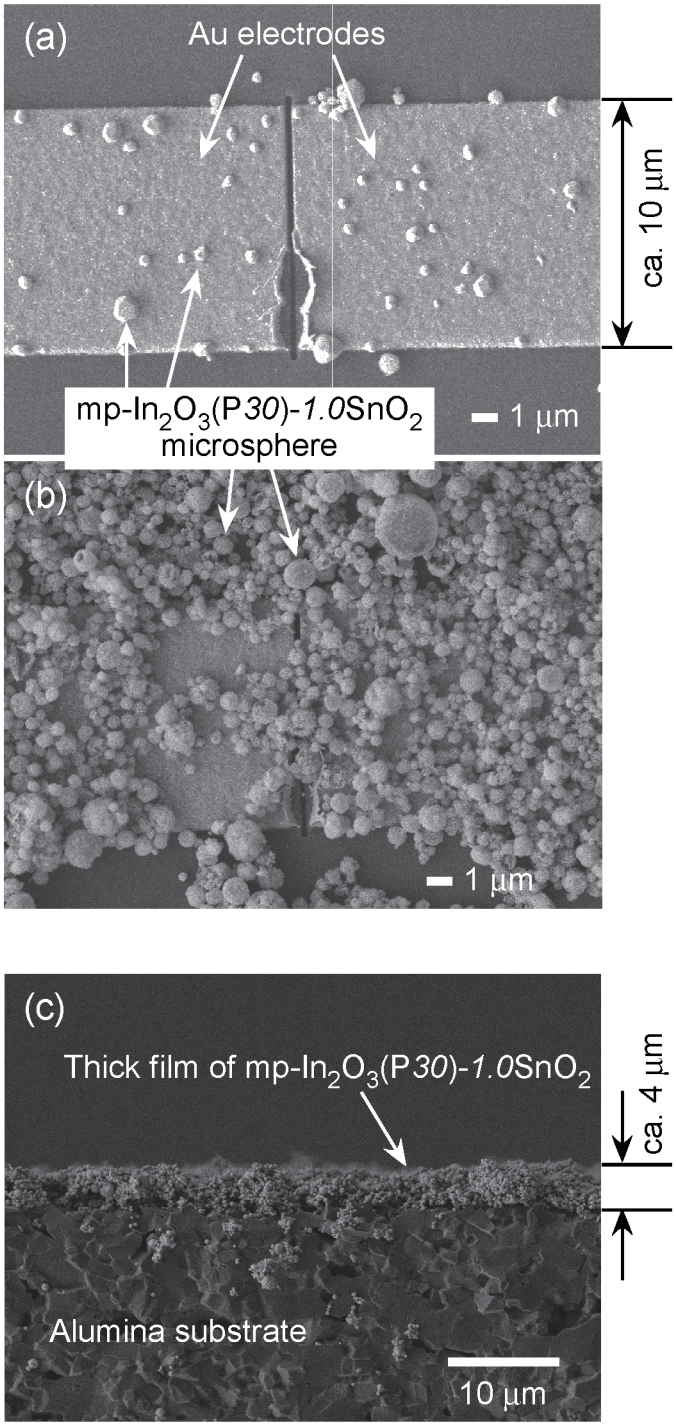

Fig. 12. SEM photographs of a surface of nano-gap Au electrodes attached (a) without or (b) with mp-In_2O_3(P*30*)-*1.0*SnO_2 microspheres (non-stacked sensor) and (c) a cross-section of a thick film sensor fabricated by screen-printing employing mp-In_2O_3(P*30*)-*1.0*SnO_2 microspheres.

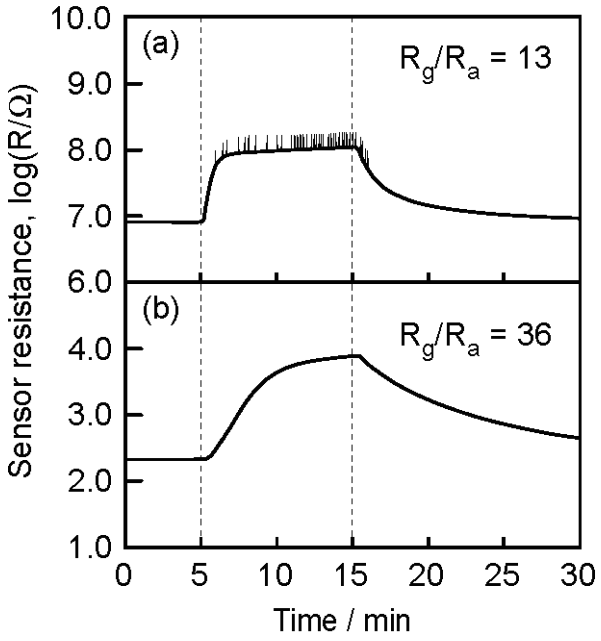

Fig. 13. Response transients to 1.0 ppm NO_2 of a non-stacked microsphere sensor and a thick film sensor of mp-In_2O_3(P*30*)-*1.0*SnO_2.

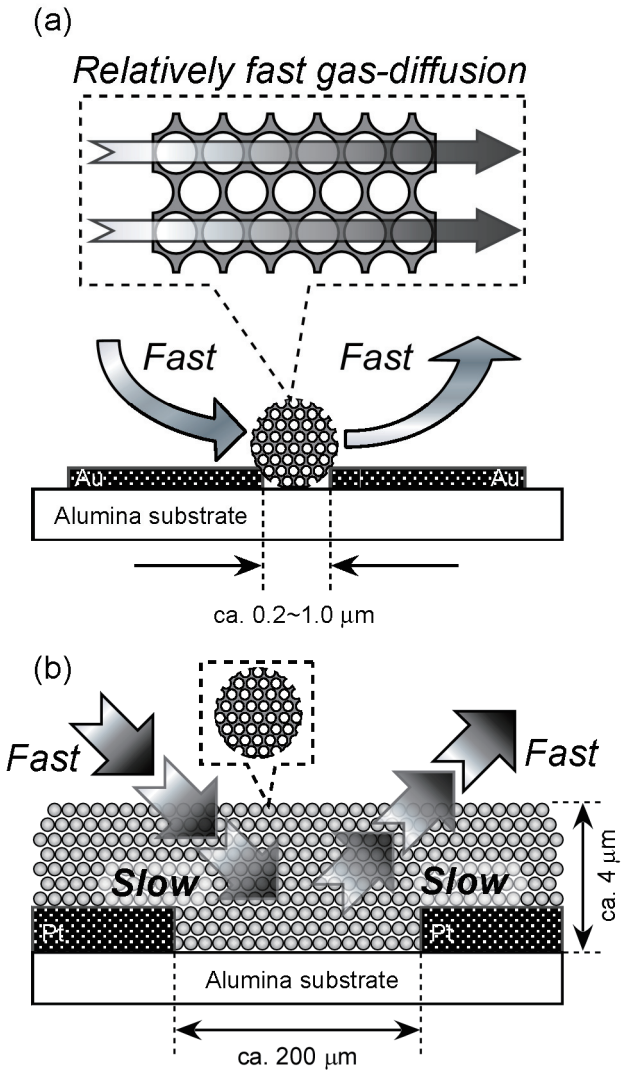

Fig. 14. Schematic drawings of gas diffusion behavior in a non-stacked microsphere sensor and a thick film sensor of mp-In_2O_3(P*30*)-*1.0*SnO_2.

Table 1. Samples prepared in this study.

Samples	Abbreviation	Symbol used in abbreviation
macroporous (mp-) In_2O_3 microspheres mixed (i) with and (ii) without SnO_2 (prepared from the precursor solution containing PMMA microspheres)	(i) mp-In_2O_3(P*m*)-*n*SnO_2	P: PMMA microspheres (ca. 150 nm in diameter) *m*: the amount of PMMA microspheres dispersed in the precursor solution (*10~30* g dm^{-3}) *n*: the amount of SnO_2 (*0.1* or *1.0* mol%)
	(ii) mp-In_2O_3(P*m*)	
conventional (c-) In_2O_3 microspheres mixed (i) with and (ii) without SnO_2 (prepared from the precursor solution containing no PMMA microspheres)	(i) c-In_2O_3-*n*SnO_2	
	(ii) c-In_2O_3	